Sn	Ti	V	Cr	Mn
	(βTi) 0-17.5% (A2) HT (αTi) 0-12.5% (A3) Ti_3Sn ($D0_{19}$) Ti_2Sn ($B8_2$) Ti_5Sn_3 ($D8_8$) βTi_6Sn_5 (hex) HT αTi_6Sn_5 (ortho)	(V) 0-16% (A2) "V_3Sn" 20-21% (A15) V_2Sn_3 (C_b=Mg_2Cu) [a])	(Cr) 0-2% (A2)	(δMn) 0-10% (A2) HT (γMn) 0-7% (A1) HT (βMn) 0-11% (A13) HT (αMn) 0-1% (A12) Mn_3Sn ($D0_{19}$) [d]) Mn_2Sn ($B8_2$) [e]) $MnSn_2$ (C16)

Fe	Co	Ni
(γFe) 0-0.8% (A1) HT (αFe) 0-9.2% (A2) Fe_5Sn_3 ($B8_2$) HT Fe_3Sn_2 (rhomb) HT FeSn (B35) $FeSn_2$ (C16)	(αCo) 0-2% (A1) HT (εCo) 0-0.2% (A3) βCo_3Sn_2 ($B8_1$) HT αCo_3Sn_2 (ortho) CoSn (B35) $CoSn_2$ (C16)	(Ni) 0-10.6% (A1) Ni_3Sn (hex) HT Ni_3Sn ($D0_{19}$) Ni_3Sn_2 (hex) HT Ni_3Sn_2 ($B8_1$) Ni_3Sn_4 (mono)

Pb	Ti	V	Cr	Mn
	(βTi) 0-16% (A2) HT (αTi) 0-4.2% (A3) Ti_4Pb ($D0_{19}$) Ti_2Pb (?)	insoluble	insoluble	insoluble

Fe	Co	Ni
insoluble	insoluble	insoluble

[a]) See also [94W2] for the composition.
[b]) Also designated as $MnSi_{2-x}$ or $MnSi_{\approx 1.7}$.
[c]) See [88Y2] for the transition temperature.
[d]) Composition range is more Mn-rich than Mn_3Sn.
[e]) Also designated as Mn_7Sn_4.
[f]) Sometimes designated as α or $\beta FeSi_2$, instead of ζ_α or $\zeta_\beta FeSi_2$.
[g]) See also [91C1] for space groups.

1.5.4.2 Ti and V alloys and compounds

Though progress is seen in thermal, structural, or electrical investigation and in high-pressure synthesis of new compounds, rather few relevant magnetic data are available. The former includes the identification of the symmetry of an ordered structure in a cubic, B1 (NaCl) type compound $TiC_{0.59}$ with carbon vacancy to be of the space group $R\bar{3}m$ [92T1], as well as new data on the lattice constants of $TiSn_2$, which are referred to in a work on resistivity measurements and listed in Table 2.

Survey

	Properties	Figure	Table
$TiSi_2$	a, b, c		2
V_3Si	$(T_1T)^{-1}$ (T), $K(T)$, $K(\chi_g)$	1, 2	
VSi_2	$\sigma_m(H)$, $\chi_m(T)$	3, 4	

Table 2. Supplement to Table 2 in LB III/19C, subsect. 1.5.4.2. Lattice constants of $TiSi_2$ [87T1].

	$TiSi_2$
Crystal structure	orthorhombic, C54
a [Å]	8.270
b [Å]	4.800
c [Å]	8.552

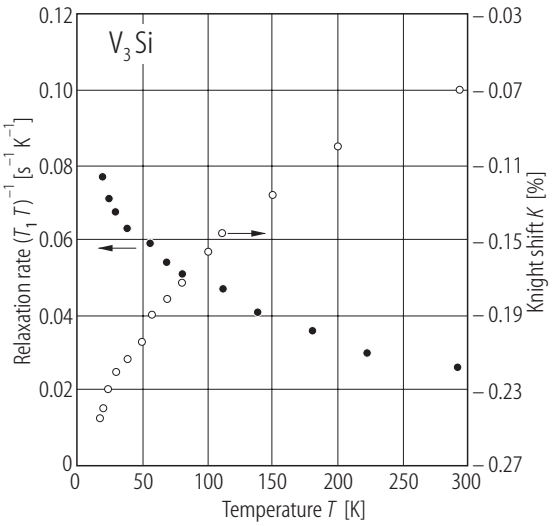

Fig. 1. V_3Si. Temperature dependence of the spin-lattice relaxation rate $(T_1T)^{-1}$ and Knight shift K of ^{29}Si [86S3].

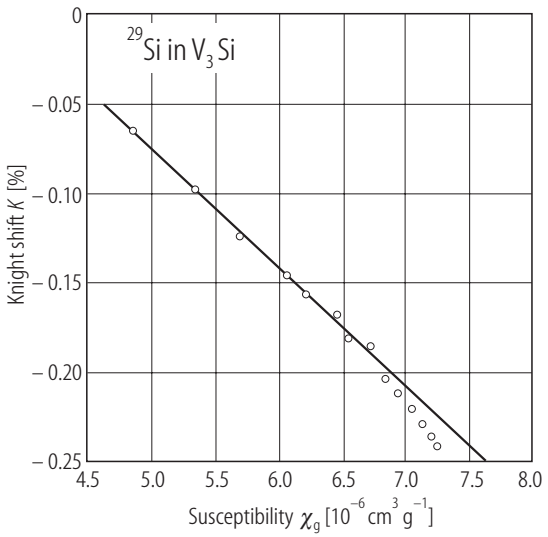

Fig. 2. V_3Si. Knight shift K of ^{29}Si vs. magnetic mass susceptibility χ_g plot [86S3].

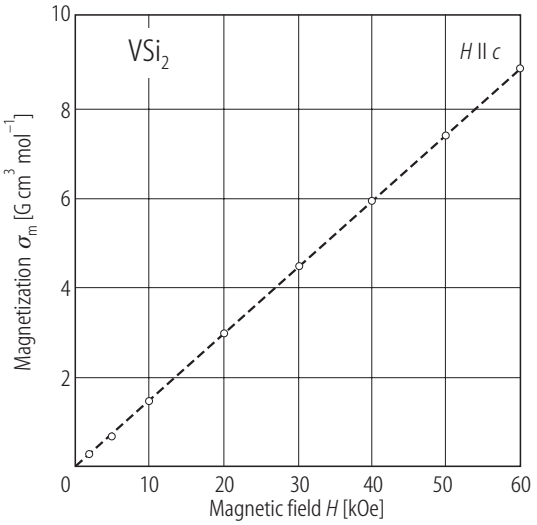

Fig. 3. VSi_2. Dependence of magnetization σ_m on an applied magnetic field H parallel to the c axis at 4 K [93G2].

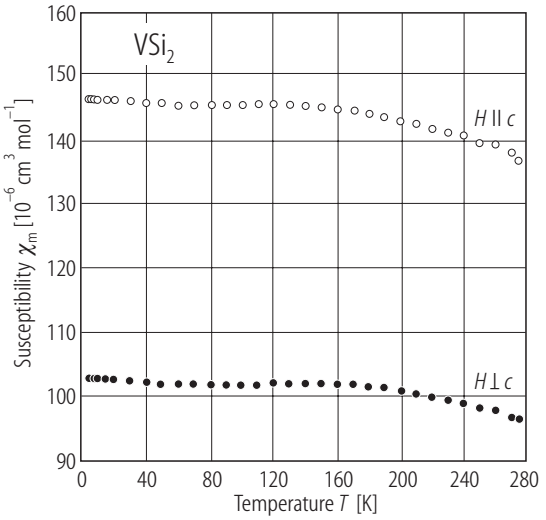

Fig. 4. VSi_2. Temperature dependence of the molar magnetic susceptibility χ_m in a magnetic field parallel or perpendicular to the c axis [93G2].

1.5.4.3 Cr alloys and compounds

Most of the work in the last decade is related to the spin-density-wave antiferromagnetism of Cr. Dilute alloys of Cr have been investigated extensively, as reviewed by [94F1]. See also subsect. 1.1.1.3 in LB III/19A.

Survey

	Composition x	Properties	Figure	Table
$Cr_{1-x}Si_x$	0.0142...0.00343	thermal expansion $\Delta l/l(T)$	5	
	0.005	$c_{ij}(T)$	6	
	0.0185	$\rho(T;p)$	7	
	0.0085	$Q(T)$	8	
	0...0.0046	x-T magnetic phase diagram	9	
$CrSi_2$		$\chi_m(T^{-1})$	10	3
$CrGe_{1-x}Si_x$	0...0.15	$\chi_g(T)$	11	
$Cr_{1-x}Ge_x$	0...0.0105	x-T magnetic phase diagram	12	
	0.0051...0.0089	p-T magnetic phase diagram	13	
$Cr_{1-x}Sn_x$	0.0007...0.0118	Mössbauer spectra	14	
	0...0.030	x-T magnetic phase diagram	15	
$(Cr_{0.987}Si_{0.013})_{1-x}V_x$	0...0.0031	thermal expansion $\Delta l/l(T)$	16	
$(Cr_{0.987}Si_{0.013})_{1-x}Mn_x$	0.0017…0.0232	thermal expansion $\Delta l/l(T)$	17	